Talanta 125 (2014) 276–283

Contents lists available at ScienceDirect

Talanta

journal homepage: www.elsevier.com/locate/talanta

Structural, nanomechanical, field emission and ammonia gas sensing properties of nitrogenated amorphous carbon films deposited by filtered anodic jet carbon arc technique

R.K. Tripathi [a], O.S. Panwar [a,*], A.K. Srivastava [b], Ishpal Rawal [a], Sreekumar Chockalingam [a]

[a] Polymorphic Carbon Thin Films Group, Physics of Energy Harvesting Division, CSIR-National Physical Laboratory, Dr. K.S. Krishnan Marg, New Delhi-110012, India

[b] Electron and Ion Microscopy, Sophisticated and Analytical Instruments, CSIR-National Physical Laboratory, Dr. K.S. Krishnan Marg, New Delhi-110012, India

ARTICLE INFO

Article history:
Received 22 January 2014
Received in revised form
26 February 2014
Accepted 5 March 2014
Available online 19 March 2014

Keywords:
Nanoindentation
Field-emission
Ammonia gas sensing
a-C: N: nc films
Nanocrystallites
Substrate bias
FAJCA

ABSTRACT

This paper reports the effect of substrate bias on the structural, nanomechanical, field emission and ammonia gas sensing properties of nitrogenated amorphous carbon films embedded with nanocrystallites (a-C: N: nc) deposited by a filtered anodic jet carbon arc (FAJCA) technique. The films are characterized by X-ray diffraction, high resolution transmission electron microscopy, energy dispersive X-ray spectroscopic analysis, Raman spectroscopy, nanoindentation, field emission and ammonia gas sensing measurements. The properties of the films obtained are found to depend on the substrate bias. The maximum hardness (H)=42.7 GPa, elastic modulus (E)=330.4 GPa, plastic index parameter (H/E)=0.129 and elastic recovery (% ER)=74.4% have been obtained in a-C: N: nc films deposited at −60 V substrate bias which show the lowest I_D/I_G=0.43, emission threshold (E_T)=4.9 V/μm accompanied with the largest emission current density (J_{max})=1 mA/cm^2 and field enhancement factor (β)=1805.6. The gas sensing behavior of the a-C: N: nc film has been tested by measuring the change in electrical resistance of the sample in ammonia environment at room temperature with the fast response and recovery time as 29 and 66.9 s, respectively.

© 2014 Elsevier B.V. All rights reserved.

1. Introduction

Over the last two decades carbon based materials, such as carbon nanotube, fullerene, diamond like carbon, amorphous carbon, graphene and so on have been investigated extensively [1–4]. Carbon exhibits a variety of crystalline and disordered structures because of its existence in three different types of hybridization: sp^3, sp^2 and sp^1. The presence of high sp^3 content is responsible for promising mechanical properties and high sp^2 content is responsible for electronic properties. These carbon based materials have been reported to show better field emission and nanomechanical properties [5,6]. Recent reports indicate that carbon materials are promising candidate for nanosized transistor [7], field emission devices [8], gas sensors [9], etc. It is well known that ammonia is a toxic gas with threshold limit value of 25 ppm for long term exposure (8 h). Ammonia is by product of decomposition of ammonium nitrate present in many explosives. However, in sensor technology inorganic materials are widely used due to their long term stability and good gas sensing behavior, but these materials have higher operating temperatures (∼200–400 °C) [10]. Ammonia sensors with room temperature operation and fast response time are highly desirable.

An enormous research has been carried out on nitrogen incorporated amorphous carbon and tetrahedral amorphous carbon (a-C: N, ta-C: N) films after the hypothetical prediction of the formation of β-C_3N_4 compound by Liu and Cohen [3,11]. The a-C: N and ta-C: N films have been formed by the bombardment of highly energetic carbon ion beam [12] and deposited by various techniques [3] such as plasma enhanced chemical vapor deposition (PECVD), sputtering, pulsed laser deposition and filtered cathodic vacuum arc (FCVA) [13–15]. As-deposited amorphous carbon (a-C) has a certain ratio of sp^3 and sp^2 carbon. The sp^3/sp^2 ratio in a-C and nitrogen incorporated a-C films with embedded nanocrystallites (a-C: nc, a-C: N: nc) is directly affected by the growth condition of films such as negative substrate bias [16], different gas atmosphere [17] and their injection method in chamber [18,19]. The sp^3/sp^2 ratios present in the films thus control the properties of a-C films. Nitrogen incorporation in a-C films leads to hard and elastic thin films which arise from the presence of nanocrystallites in amorphous matrix of carbon [17,18].

There are established theoretical [20] and experimental [21] methods for the formation of different carbon nanostructures such as carbon nanotube and fullerene by arc discharge. Amaratunga et al.

* Corresponding author. Tel.: +91 11 45609175; fax: +91 11 45609310.
E-mail address: ospanwar@mail.nplindia.ernet.in (O.S. Panwar).

http://dx.doi.org/10.1016/j.talanta.2014.03.005
0039-9140/© 2014 Elsevier B.V. All rights reserved.

[21,22] reported the deposition of hard and highly elastic carbon films which consist of graphitic sp^2 bonding using a graphite cathode with localized high pressure of helium or nitrogen at the arc spot. Depending upon whether the gas is injected through the cathode or anode, the technique will be termed as cathodic jet carbon arc (CJCA) or anodic jet carbon arc (AJCA). Based on the high pressure arc plasma methods developed to produce fullerene molecules and nanotubes [21], we have used a high local nitrogen gas pressure using AJCA technique for thin film deposition in presence of a magnetic field. Alexandrou et al. [23] have synthesized a-C: N films with nanoparticles deposited by unfiltered AJCA technique. With the high rate of ionization and the option to vary the ion energy and ion density, under optimum conditions it can lead to the creation of momentary pseudo-thermodynamic conditions of high temperature on the surface of film, which leads to formation of nanostructured carbons [24]. The main objective of the present study is to investigate the effect of substrate bias on the structural, nanomechanical, field emission of a-C: N: nc films deposited using FAJCA technique. Further, we report ammonia gas sensing at room temperature with fast response and recovery time in a-C: N: nc films and correlate with their field emission display applicability. For comparison purpose, we also refer the properties of ta-C: N films deposited using the S bend FCVA process [15,25] and a-C: N films with embedded nanocrystallites deposited using FCJCA technique [18].

2. Experimental

2.1. Sample preparation

The FAJCA process is based on striking the arc (arc voltage ~20–24 V with an arc current of ~56 A) between two graphite electrodes (50 mm dia. graphite cathode of purity 99.999% and a retractable graphite anode rod of 7 mm dia. and purity 99.999%). The linear magnetic filter which was used for the removal of macroparticles generated in the arc was energized using direct current (D.C.) power supply and a magnetic field of ~350 G is achieved inside the duct. The chamber was initially pumped to a base pressure of $\sim 10^{-6}$ mbar by the use of turbo-molecular and rotary pump combination in the system and then the high purity (99.999%) nitrogen gas was injected locally through the anode of 1 mm cavity. The a-C: N: nc films were deposited on cleaned 7059 glass substrate and highly doped $<100> n^{++}$ silicon substrates, placed at a distance of ~35 cm away from the cathode, at a nitrogen pressure of $\sim 8.6 \times 10^{-3}$ mbar. An additional negative substrate bias (direct current) ranging from 0 to −300 V was applied to the substrate to enhance the energy of the incoming ions. The films studied were deposited sequentially for 5 s and then cooled for 50 s. The process was repeated in order to obtain the required thickness. The thicknesses of the films were in the range 180 ± 10 nm as measured by a Talystep (Rank Taylor and Hobson) thickness profiler. The deposition rate achieved was in the range 0.5–0.7 nm/s with 60 A arc current for the growth of a-C: N: nc films. Other details of the system are already published elsewhere [19].

2.2. Characterization of samples

The phase analysis of the films was carried out by a Rigaku Miniflex-II diffractometer using CuKα radiation at room temperature which was fully automated and configured in 0–2θ geometry. The high-resolution transmission electron microscope (HRTEM) (Model FEI, Tecnai G2 F30-STWIN with field emission electron gun source) was operated at the electron accelerating voltage of 300 kV to explore the nano- and sub-nano-scale structural information present in these films. For HRTEM samples, the a-C: N: nc films coated on silicon substrates were immersed in $HF+HNO_3$ mixtures which etched away Si substrates. On dilution of the mixtures with distilled water, the a-C: N: nc film floats on the surface of water. Subsequently, these self-supported films were lifted on a 200-mesh copper grid of 3.05 mm in diameter. The nanomechanical properties of the films were measured using IBIS nanoindentation (Fisher-Cripps Laboratories Pvt. Ltd., Australia) using Berkovich indenter at maximum 3 mN load. The field emission measurements were carried out using parallel plate configuration using a high voltage source meter (Keithley model 2410). An indium tin oxide coated glass was used as anode and a-C: N: nc films deposited on polished silicon substrate as cathode. The separation between the electrodes is defined by a pTFE spacer of thickness ~50 μm and the overlap area between the plate anode and cathode was kept at 0.196 cm^2. The current voltage (I–V) characteristics were measured at room temperature in a vacuum $\sim 2.5 \times 10^{-7}$ mbar maintained by a turbomolecular rotary pump based vacuum system. The emission current density (J) is calculated by dividing the emission current by the area of the cathode which is defined by area of the hole in spacer. The electric field (E) is obtained by voltage drop across the vacuum gap. Gas sensitivity measurements were performed in a fully automated system on the film by using Keithley's 2000 digital multimeter and a Alicat mass flow controller.

3. Results and discussion

3.1. XRD study

Fig. 1 shows the typical X-ray diffraction of a-C: N: nc film deposited at −60 V substrate bias. XRD pattern shows a broad peak at 28° accompanied with a broad shoulder centered at ~43°. This indicates that the deposited film is found to be dominantly amorphous in nature but nanocrystallites are embedded in the amorphous matrix [JCPDS file no. 75-0623] [26]. Similar patterns were observed in a-C: N: nc films deposited at different substrate biases.

3.2. HRTEM study

Fig. 2(a) shows the overall film microstructure with the varied gray contrast. These contrasts are evolved due to the various grain boundaries and crystallinity associated at different regions at atomic scale. A further high magnification in Fig. 2(b) clearly delineates to distinct region of crystalline zone (marked as A) embedded in the overall amorphous structure of the film. A particular region of amorphous matrix separating the crystalline region has been denoted as B (in Fig. 2(b)). Several such regions

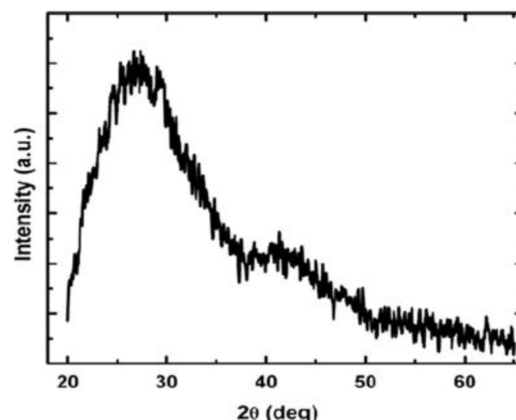

Fig. 1. Typical X-ray diffraction patterns of a-C: N: nc film deposited at −60 V showing dominantly amorphous structure.

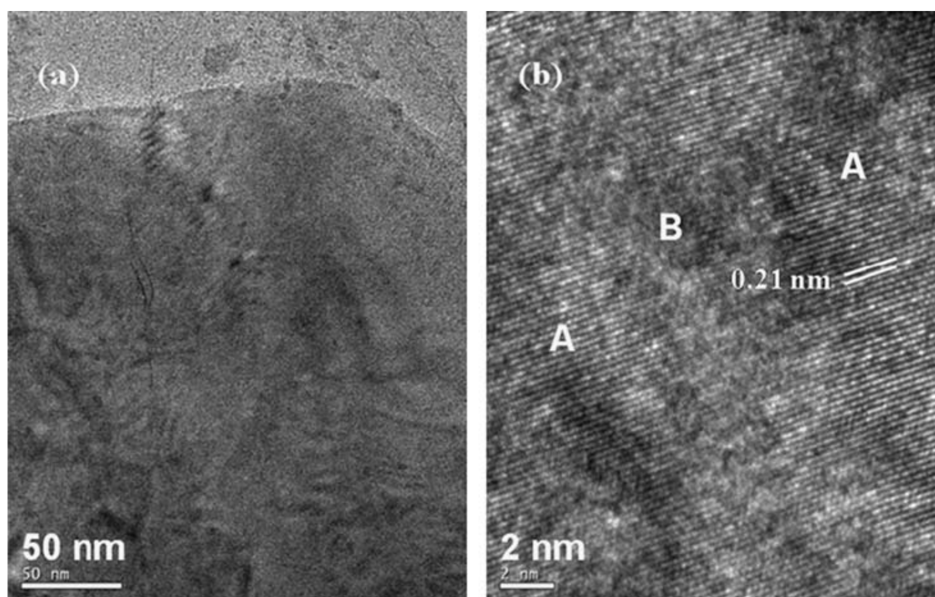

Fig. 2. (a and b) HRTEM micrographs showing the distribution of ultrafine nanocrystallites of a-C: N: nc film deposited at −60 V substrate bias.

were explored during the electron microscopy experiment and realized that in general the film is constituted of amorphous phase with coexisting ultrafine nanocrystallites.

3.3. EDAX study

Fig. 3 shows the typical energy dispersive X-ray spectroscopic analysis (EDAX) spectra of a-C: N: nc film deposited at −60 V substrate bias. The EDAX pattern of a-C: N: nc film shows strong Si peak in addition to the low intensity C and N peaks. The strong Si peak observed in the spectra is attributed to the fact that Si substrate was used for the growth of a-C: N films. The N content estimated in the film is found to be ~6.8 at.%. Hu et al. [27] reported that carbon nitride materials containing up to 12 at.% nitrogen can be grown without the reduction in the percentage of sp^3-bonded carbon. Further increase in the nitrogen composition, however, produced a structural transformation to carbon nitride materials in which carbon showed predominantly sp^2 bonding. The a-C: N: nc film deposited in the presence of nitrogen gas with varying negative substrate bias in the present study exhibits the nanocrystallites of diamond (sp^3-bonded carbon) as recorded by the HRTEM image (Fig. 2(b)).

3.4. Raman spectroscopy

The Raman spectra together with the deconvoluted Raman spectra of a-C: N: nc films deposited at different substrate biases in the wave number range from 1100 to 1900 cm^{-1} are shown in Fig. 4(a–d). It is evident from the figure that the spectra show a broad peak at around 1563–1575 cm^{-1} and a shoulder at about 1402–1422 cm^{-1}. Thus, the a-C: N: nc films exhibit two bands: D (disorder) band at 1412 ± 10.5 cm^{-1} and G (graphite) band at 1569 ± 6 cm^{-1}. The values of G band peak position, full width at half maximum of G band (FWHM-G), D band peak position, FWHM-D and intensity ratio of D band to G band (I_D/I_G) obtained in a-C: N: nc films at different negative substrate biases have been summarized in Table 1. The a-C: N: nc film deposited at 0 V substrate bias showed G band at 1564.9 cm^{-1} with FWHM-G of 132.6 cm^{-1} and shoulder (D band) at ~1391.9 cm^{-1} with FWHM-D of 237.7 cm^{-1} accompanied with $I_D/I_G=0.63$. The a-C: N: nc films showed shift in D band to higher wave number and G band to lower wavenumber accompanied with the increase in FWHM of

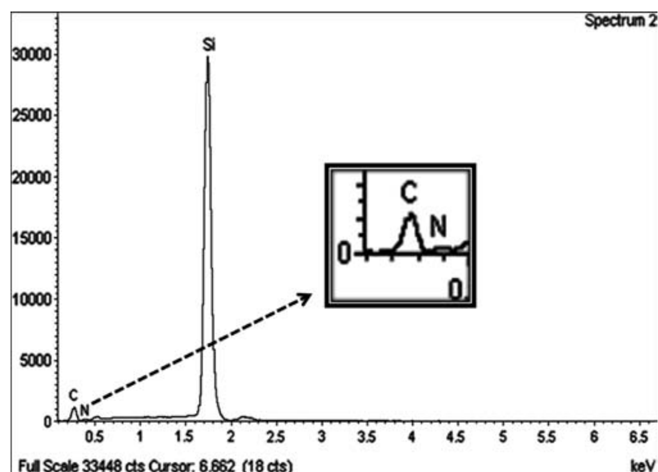

Fig. 3. Typical EDAX spectra of a-C: N: nc film deposited at −60 V substrate bias.

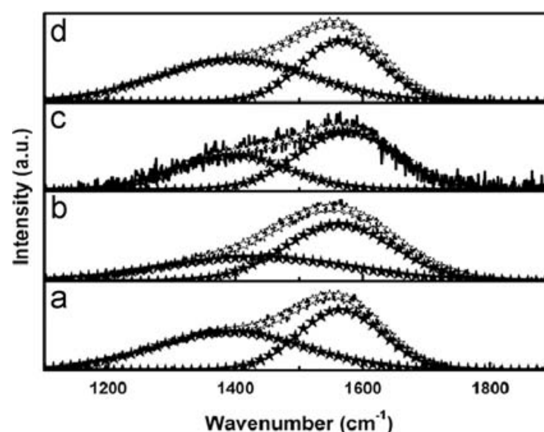

Fig. 4. Raman spectra and deconvoluted spectra of a-C: N: nc films deposited at different negative substrate biases of (a) 0 V, (b) −60 V, (c) −150 V and (d) −300 V in the wave number range from 1100 to 1900 cm^{-1}.

G and D bands and decrease of I_D/I_G ratio with the increase of substrate bias. Beyond −60 V substrate bias, there is a reversal in the trend where I_D/I_G ratio starts increasing. It is well known that

Table 1
Various parameters evaluated from the Raman spectra of a-C: N: nc films deposited at different negative substrate biases.

Substrate bias (V) Properties	0	−60	−150	−300
D (cm^{-1})	1391.9	1432.4	1393.8	1398.4
G (cm^{-1})	1564.9	1562.9	1575.1	1566.4
FWHM-D (cm^{-1})	237.7	293.9	177.0	244.5
FWHM-G (cm^{-1})	132.6	175.0	156.7	130.3
I_D/I_G	0.63	0.43	0.59	0.69

Raman scattering is a resonance process in which those configurations whose band gap match the excitation energy are preferentially excited. Visible Raman spectroscopy is 50–230 times [28,29] more sensitive to sp^2 sites than sp^3 sites because visible photons (2.2 eV) preferentially excite the π states. Therefore, visible Raman spectroscopy is able to probe only the sp^2 sites. It depends fundamentally on the ordering of sp^2 sites and only indirectly on the fraction of sp^3 sites [30]. Therefore, the use of visible excitation source at 514.5 nm for the Raman measurements restricts the estimation of sp^3 fraction to indirect means like hump at around 1360–1450 cm^{-1} as D band and G peak whose position shifts and the width indicate the relative concentration of sp^2 bonded carbon and the nature of carbon cluster in the film [3,30,31]. The band positions obtained in a-C: N: nc films are well matched with the band position observed by other group [3,30]. The deconvoluted Raman spectra show two Gaussian peaks after subtraction of the background from the spectra by linear method and are associated with their microstructures with the G band at around 1560–70 cm^{-1} due to symmetric E_{2g} C–C structure mode disordered graphite and D band at around 1380–1430 cm^{-1} presumably due to bond angle disorder in micro-domains affected by sp^3 bonds of diamond [30]. For the indirect qualitative evaluation of the amount of the sp^3 and sp^2 contents present in the films, the intensity ratio of the D band to G band (I_D/I_G) has been evaluated [30]. The minimum value of I_D/I_G=0.43 is evaluated in a-C: N: nc film deposited at −60 V substrate bias which indicates that the sp^3 content is maximum in a-C: N: nc film deposited at −60 V substrate bias.

3.5. Nanoindention study

High resolution nanoindentation was used to measure the nanomechanical properties of a-C: N: nc films. The load versus displacement curves for a-C: N: nc films deposited at different substrate biases of (a) 0 V, (b) −60 V, (c) −150 V and (d) −300 V are shown in Fig. 5. These load versus displacement curves suggested that one can roughly estimate the hard and super hard behavior of coatings. From all the curves, it is evident that the a-C: N: nc film deposited at −60 V substrate bias (Fig. 5(b)) has very small hysteresis between loading–unloading curves with a significant recovery during unloading which reveals super hard behavior. The films deposited at other substrate biases having hard characteristic [Fig. 5(a), (c) and (d)] exhibit comparatively broader hysteresis between loading–unloading curves with lesser recovery during unloading cycle in comparison to Fig. 5(b). Sjostrom et al. [32] have reported this kind of narrow hysteresis between loading–unloading curve with high recovery in super hard and elastic carbon nitride thin film. Thus, the a-C: N: nc film deposited at −60 V substrate bias may have super hard characteristic, but direct estimation of other nanomechanical parameters such as hardness (*H*), elastic modulus (*E*), plastic index parameter (*H*/*E*) and % elastic recovery (% *ER*) are also very important to confirm this behavior. % *ER* in these a-C: N: nc films was estimated to elucidate elastic properties using the relation

$$\% ER = \frac{(h_{max} - h_{res})}{h_{res}} \times 100 \qquad (1)$$

where h_{max} and h_{res} are the displacement at maximum load and residual displacement after load removal, respectively. Fig. 6 shows the variation of *H*, *E*, % *ER* versus negative substrate bias. It is evident from the figure that the values of *H*, *E* and % *ER* of the films vary in range from 22.3 to 42.7 GPa, 275 to 330 GPa and 48.6 to 74.4, respectively. The values of *H*, *E* and % *ER* of a-C: N: nc films initially increased with the increase of substrate bias from 0 to −60 V. Beyond −60 V, there is a reversal in the trend. The maximum value of *H*, *E* and % *ER* in the film deposited at −60 V substrate bias were found to be 42.7 GPa, 330.03 GPa and 74.4, respectively. Sjostrom et al. [32] have observed super hard behavior in carbon nitride films having 85% elastic recovery. Fallon et al. [13] obtained maximum sp^3 bonding at about 100 eV in ta-C films deposited using FCVA technique beyond (>100 eV) which initiation of graphite-like sp^2 bonding has been observed.

The *H*/*E* was found to be an important parameter to explain elastic–plastic and wear resistance properties of thin films [6]. The *H*/*E* ratio shows the physical response of an atomic lattice to an external force and relates to the bulk fracture strength. For high wear resistance coatings, the *H*/*E* must be very high. Thus, films having even comparatively lower *H* but having higher *H*/*E* can be very useful for high wear resistance coating on magnetic storage media and other applications [6]. To explore elastic and plastic properties of these a-C: N: nc films in term of energy, the plastic deformation energy (U_r) has also been estimated using an empirical formula [33]

$$U_r = \left[\frac{1}{3}\sqrt{\frac{1}{\omega_0 \tan^2\Psi}}\right]\frac{1}{\sqrt{H}}P^{3/2} \qquad (2)$$

where, ω_0 is the geometry constant that attains the value of 1.3 for pyramid indenter, *P* is the load, and Ψ is the half angle of Berkovich indenter that has the value of 65.3. The deformation energy (U_r) varies inversely with *H*. Fig. 7 shows the variation of *H*/*E* and U_r evaluated in a-C: N: nc films versus negative substrate bias. The values of *H*/*E* and U_r are found to be in the range between 0.08 and 0.13 and 1.06×10^{-11} and 1.47×10^{-11} J, respectively. It is evident from the figure that the values of *H*/*E* increased and those of U_r decreased with the increase of substrate bias up to −60 V and beyond −60 V there is a reversal in the trend. The maximum value of *H*/*E* of 0.13 accompanied with the minimum value of U_r of 1.06×10^{-11} J was obtained in a-C: N: nc film deposited at −60 V which again revealed their high wear resistant capability accompanied with less plastic (high elastic) deformation and more diamond nature of film. Lin et al. [34] have suggested that U_r varies inversely with % *ER*. The U_r results obtained in the present study are found to be in good agreements with *H* and % *ER* results.

The penetration depth at 3 mN in all the a-C: N: nc films was found to be in the range between 58 and 79 nm. Mostly, nanomechanical characterization should be performed within 10–25% of the film thickness. In the present study, the indentation depths in all the a-C: N: nc films have crossed the limit, so the substrate also influences the mechanical properties and the result showed composite substrate/film effect. Although, due care was taken here to avoid the effect of substrate, but we were unable to completely avoid it as the thickness of these films was not very high. However, because of this, the hardness of Si wafer was measured before the deposition and then hardness of substrate/film was estimated by composite hardness model [35]. The effect of substrate on the mechanical properties of thin films has also been studied in the literatures [36,37]. They have considered two different cases of soft film on hard substrate and hard film on soft substrate.

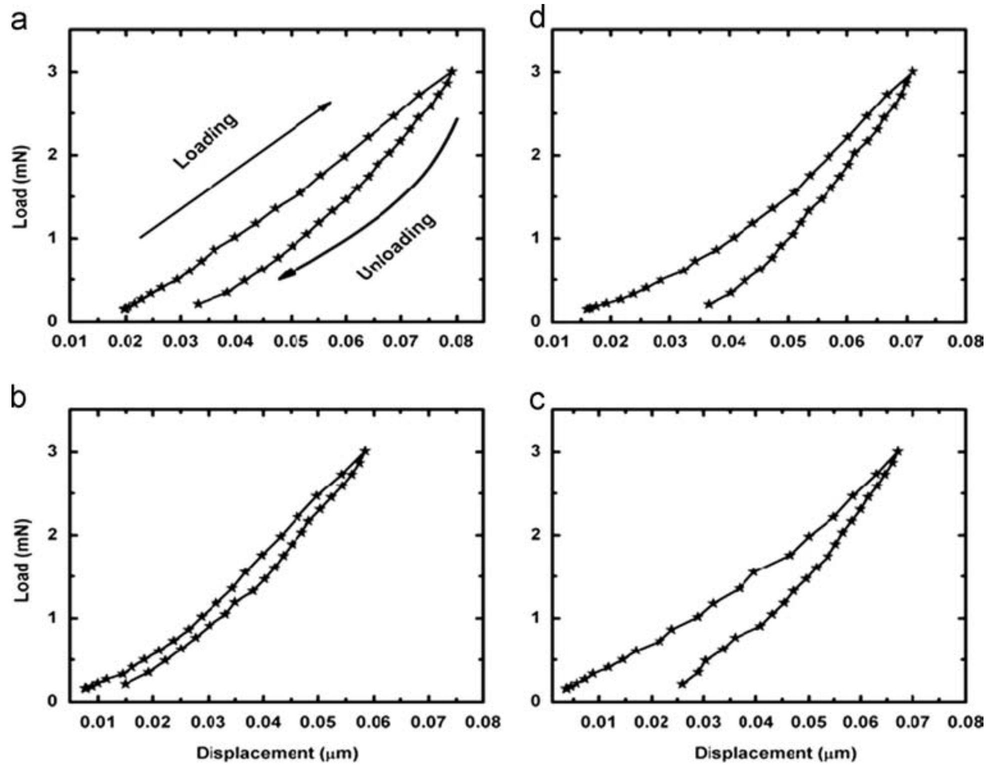

Fig. 5. Load–displacement curves of a-C: N: nc films deposited at different negative substrate biases of (a) 0 V, (b) −60 V, (c) −150 V and (d) −300 V.

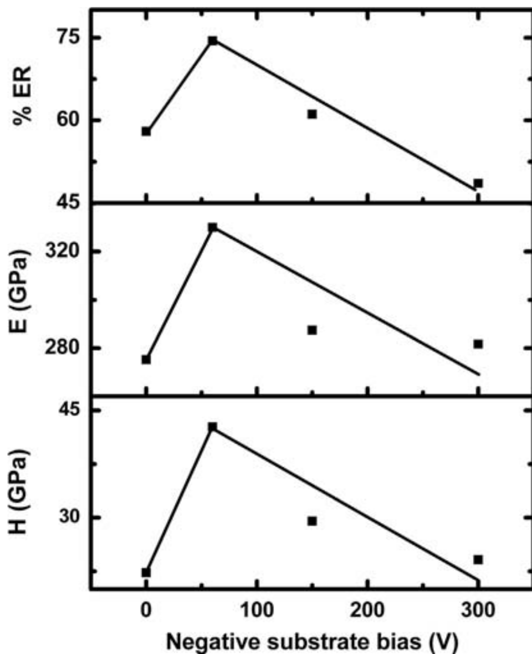

Fig. 6. Variation of H, E and % ER of a-C: N: nc films versus negative substrate biases.

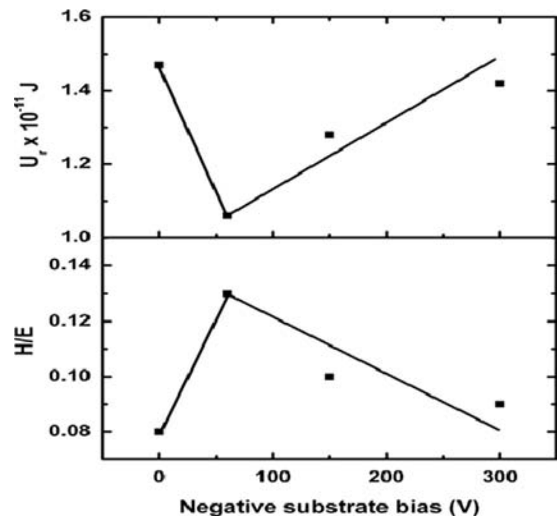

Fig. 7. Variation of H/E and U_r of a-C: N: nc films versus negative substrate biases.

They have realized that hard film on soft substrate exhibited decrease in hardness with the increase in penetration depth. The hardness values of a-C: N: nc films in the present study are found to be larger than the hardness value of silicon substrate which belongs to the latter case discussed. It may be due to the effect of soft silicon substrate. The value of hardness reported in the present study might be a lower value whereas the actual value of hardness may be larger than the reported value [35].

Zhang et al. reported the effect of load on the mechanical properties of a-C films [38]. They suggested that with increasing the load, the plasticity in the structure of film increases due to the substrate effect, which means the decrease of elastic recovery and hardness values. We also performed nanoindentation study with increasing indentation load from 3 to 9 mN and found that the values of H and E decrease for the case of hard film on soft substrate in the present study.

3.6. Field emission study

Fig. 8 shows the variation in field emission current density (J) versus electric field (E) characteristics of a-C: N: nc films deposited at different negative substrate biases. Field-emission involves a

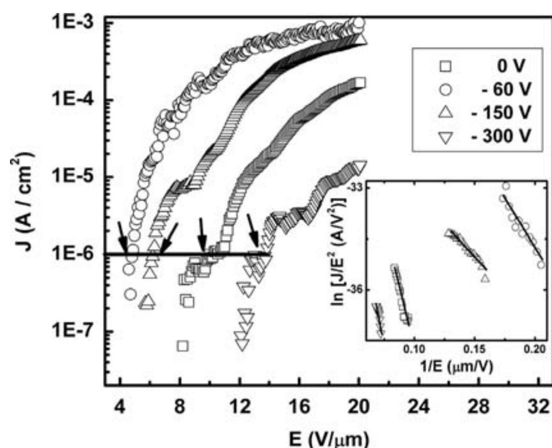

Fig. 8. Variation in field emission current density (J) versus electric field (E) characteristics of a-C: N: nc films deposited at different negative substrate biases. Inset shows their FN plots.

Table 2
Various emission parameters of a-C: N: nc films deposited at different negative substrate biases.

Substrate bias (V) Properties	0	−60	−150	−300
E_T (V/μm)	10.0	4.9	6.3	13.8
J_{max} (mA/cm^2)	0.17	1.0	0.59	0.01
ϕ (β=1)	0.076	0.034	0.036	0.086
β (ϕ=5 eV)	525.8	1805.6	1597.5	439.3

quantum-mechanical process in which electrons tunnel out of the electrodes into vacuum when subjected to a very high electric field. It is a non-linear process, in which the J–E characteristics are usually described by the classical Fowler–Nordheim (FN) equation [39,40]

$$J = A[(\beta E)^2/\varphi]\exp(-B\varphi^{3/2}/\beta E) \quad (3)$$

where J is the current density, φ is the barrier height (taken as the work function), E is the applied electric field, β is the field enhancement factor and A and B are constants and have the values of 1.54×10^{-6} A V^{-2} and 6.83×10^{9} Vm^{-1}eV$^{-3/2}$, respectively. The plots of log (J/E^2) versus $1/E$ for the corresponding J–E characteristics are shown in the inset of Fig. 8. These plots are straight lines which confirm that the J–E characteristics follow the FN relation. The threshold field of emission (E_T) is defined as the applied electric field at which an emission current density (J) of $\sim 1\times 10^{-6}$ A/cm^2 is obtained and is shown by the arrow in each curve. The slopes of these plots give the effective emission barriers ϕ, if we assume as ideal plane emitter with a field enhancement factor β of 1. The values of ϕ for a-C: N: nc films grown were in the range of 0.034–0.086 eV. Other workers [24,41–44] reported similar values of ϕ. These values are obviously quite low and the true barrier may be large [45]. If we take a work function (ϕ) of 5 eV, typical of graphite bonding, then the FN plots correspond to the field enhancement factor β of 439.3–1805.6 for these a-C: N: nc films. The values of E_T, J_{max} at 20 V/μm, ϕ and β of a-C: N: nc films are summarized in Table 2. The values of E_T=10 V/μm accompanied with J_{max}=0.17 mA/cm^2 and β=525.8 have been obtained in a-C: N: nc film deposited at 0 V substrate bias. The value of E_T decreases to 4.9 V/μm and those of J_{max} and β increase to 1.0 mA/cm^2 and 1805.6, respectively, on the application of substrate bias of −60 V. Beyond −60 V substrate bias, there is a reversal in the trend and the value of E_T increases and those of J_{max} and β decrease. The decrease of E_T is correlated with the increase of sp^3 content present in a-C: N: nc film deposited at −60 V substrate bias. Beyond −60 V substrate bias, the value of E_T increases and the sp^3 content decreases. The E_T of 4.9 V/μm accompanied with the largest J_{max} of 1 mA/cm^2 and β of 1805.6 are obtained in a-C: N: nc film deposited at −60 V substrate bias which showed maximum values of sp^3 content corresponding to the minimum I_D/I_G ratio in the Raman spectra.

There are various other factors which influence field emission. A satisfactory field-emission behavior of the a-C films can be expected from the presence of both graphitic and diamond-carbon components. There may also be an optimum abundance ratio and connectivity of the network of diamond and graphitic carbon in the films where these films may perform as better field-emitters. Gupta et al. [46], while studying the electron field-emission and microstructure correlation in nanocrystalline carbon thin films, stated that along with grain size and optical band gap dependence, the defects play a crucial role and assist in lowering emission threshold. We reported [41,42] a correlation of E_T in diamond like carbon (DLC) films grown by various techniques on residual stress, optical band gap (E_g), and characteristic energy of band tails (Urbach energy, E_0) and the values of E_T decrease with the decrease of residual stress, E_g and E_0, as well. It is also evident from the field emission study of a-C films having embedded nanocrystallites deposited under different gaseous environment by FCJCA technique [47] that low E_T is obtained in those films that have high sp^3 content, low H/N content, high surface roughness and smaller size of nanocrystallite. Various other process parameters such as substrate temperature [48] and surface treatment by plasma etching [49] substantially affect in enhancing the graphitic content which enhances the emission current density. Koinkar et al. [50] suggested that the presence of nanocrystalline diamond crystallites on the microcrystalline grains offers higher aspect ratio which is responsible for the observed decrease in the threshold field values. Electrical conductivity is an important factor which also influences the emission behavior. Several review articles on field emission [3,8,51] are also available in the literature.

3.7. NH_3 sensing study

The gas sensing response in a-C: N: nc film in the ammonia environment is originated due to the electron donating nature of ammonia which changes the charge carrier concentration in a-C: N film and hence we get the change in the electrical resistance of the a-C: N: nc film. This change in electrical resistance or the sensitivity of the sensor depends upon the process of charge carrier neutralization. The same process is adopted for all two cycles at 50 ppm and all five cycles from 50 to 300 ppm of ammonia. All the measurements were performed on the same a-C: N: nc film. The film was tested for seven cycles (two at 50 ppm and five at 50–300 ppm) of measurement which indicates the high sensitivity and reusability of the film. Fig. 9(a) exhibits the sensing behavior of a-C: N: nc film deposited at −60 V substrate bias at room temperature with fix 50 ppm of ammonia gas. The operation of this sensor is based on the reversible change of electrical resistance on exposure to ammonia gas. It is evident from the figure that the electrical resistance almost recovered after one complete cycle of ammonia gas at fix 50 ppm level. Fig. 9 (b) shows the fitting of the conductance for response and recovery of a-C: N: nc film sensor in the presence of 50 ppm ammonia at room temperature. The solid lines for response and recovery are calculated using

$$G(t)_{response} = G_0 + G_1[\exp(-t/\tau_{response})] \quad (4.i)$$

and

$$G(t)_{recovery} = G_0 + G_1[\exp(-t/\tau_{recovery})] \quad (4.ii)$$

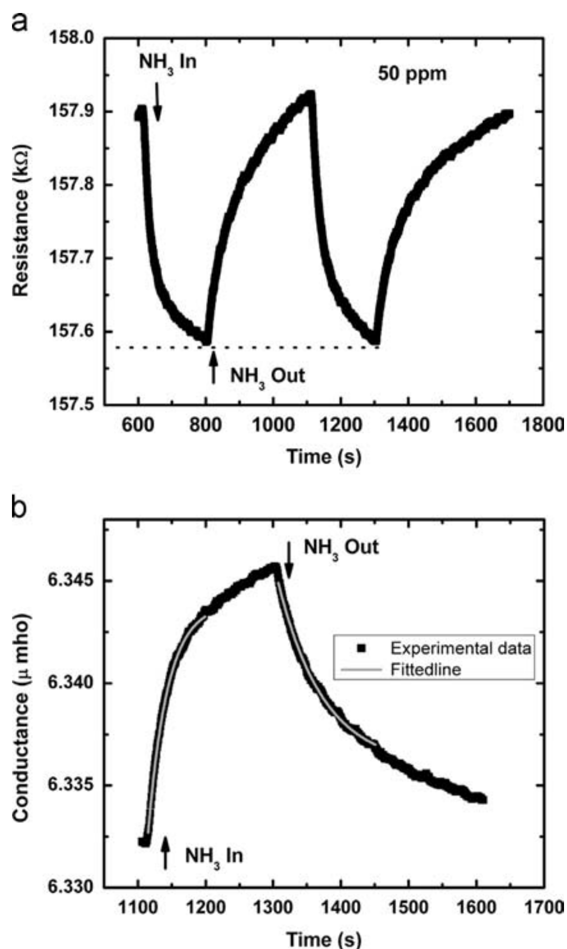

Fig. 9. (a) Change in resistance at 50 ppm of ammonia gas and (b) fitting of the change in conductance for response and recovery time at 50 ppm levels of ammonia gas for a-C: N: nc film deposited at −60 V substrate bias.

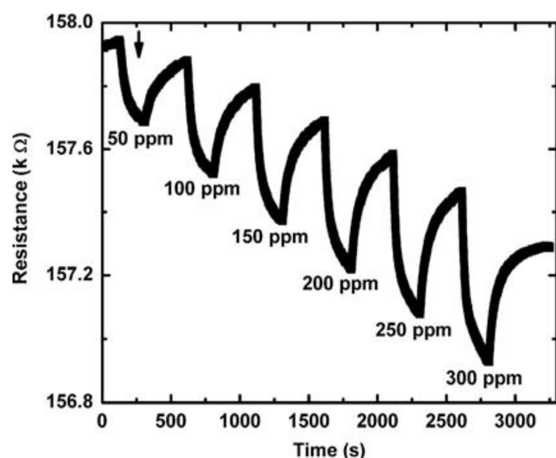

Fig.10. Change in resistance at 50–300 ppm of ammonia gas for a-C: N: nc film deposited at −60 V substrate bias.

where G_0 and G_1 are fitting parameters with $\tau_{response}$ and $\tau_{recovery}$ as the response and recovery time of ammonia sensor. Fig. 10 shows the gas sensing of a-C: N: nc film with increasing level from 50 to 300 ppm of ammonia. The calculated sensor response varies from 0.1 to 0.4 for 50–300 ppm level of ammonia. Recently, Au decorated carbon nano-tubes (CNTs) have been used for room temperature sensing of ammonia gas [52]. However, this method is not cost effective due to the use of gold nanoparticle. Pandey et al. [53] developed a very simple cost effective technique for the room temperature ammonia sensing by guar gum/silver nanoparticles composite. They claimed that the sensor based on guar gum/silver nanoparticles composite was flexible and ultrasensitive for ammonia gas. Hu et al. [54] reported the use of chemically reduced graphene oxide as room temperature ammonia sensor. A major issue with this method is that an additional IR lamp is required for recovery which increases the complexity of sensor. The use of zinc oxide and functionalized graphite and multi-walled CNTs for room temperature ammonia sensing has also been reported with the slow response and recovery time compared with other CNT based sensors [55]. Karunagaran et al. [56] while investigating TiO_2 thin film gas sensor for monitoring ammonia gas have reported the response time of 90 s and recovery time 110 s for 500 ppm NH_3 in air at 250 °C.

4. Conclusion

The effect of negative substrate bias on the structural, nano-mechanical and field emission properties of a-C: N: nc films deposited by FAJCA technique have been studied. The properties are found to depend on the substrate bias applied and peak at −60 V substrate bias. Maximum values of H of 42.7 GPa, E of 330 GPa, H/E of 0.13, % ER of 74.4, J_{max} of 1 mA/cm^{2}and β of 1805.6 with the lowest value of E_T of 4.9 V/μm have been obtained in a-C: N: nc films deposited at −60 V substrate bias. The formation of a-C: N: nc films may have the potential to be a thin film equivalent of carbon nanotubes in terms of mechanical properties and may act as better performing hard carbon coating materials. It also demonstrates a better field emission behavior and good response and recovery time in ammonia sensing at room temperature.

Acknowledgments

The authors are grateful to Prof. R.C. Budhani, Director, CSIR-National Physical Laboratory, New Delhi (India) for his kind permission to publish this work. We thank to Mr. K.N. Sood for providing EDAX spectra, to Dr. V.P.S. Awana for providing XRD pattern and to Dr. Sushil Kumar for useful discussion. Mr. R.K. Tripathi is grateful to the Department of Science and Technology, Ministry of Science and Technology and Ministry of New and Renewable Energy, Government of India for providing the financial assistance during the course of this work.

References

[1] A.K. Geim, K.S. Novoselov, Nat. Mater. 6 (2007) 183–191.
[2] Z. Sun, Z. Yan, J. Yao, E. Beitler, Y. Zhu, J.M. Tour, Nature 468 (2010) 549–552.
[3] J. Robertson, Mater. Sci. Eng. R 37 (2002) 129–281.
[4] P.K. Chu, L. Li, Mater. Chem. Phys. 96 (2006) 253–277.
[5] J.D. Carey, R.D. Forrest, S.R. P. Silva, Appl. Phys. Lett. 78 (2001) 2339–2341.
[6] C.A. Charitidis, Int. J. Refract. Met. Hard Mater. 28 (2010) 51–70.
[7] W. Lu, C.M. Lieber, Nat. Mater. 6 (2007) 841–850.
[8] J.D. Carey, R.C. Smith, S.R. P. Silva, J. Mater. Sci.: Mater. Electron. 17 (2006) 405–412.
[9] J.W. Han, B. Kim, J. Li, M. Meyyappan, RSC Adv. 4 (2014) 549–553.
[10] L. Yuan, T. Hyodo, Y. Shimizu, M. Egashira, Sensors 11 (2011) 1261–1276.
[11] Y. Liu, M. Cohen, Science 245 (1989) 841–842.
[12] J.G. Buijnsters, M. Camero, L. Vazquez, F.A. Rueda, C.G. Aleixandre, J.M. Albella, Vacuum 81 (2007) 1412–1415.
[13] P.J. Fallon, V.S. Veerasamy, C.A. Davis, J. Robertson, G.A.J. Amaratunga, W.I. Milne, J. Koskinen, Phys. Rev. B 48 (1993) 4777–4782.
[14] O.S. Panwar, B. Deb, B.S. Satyanarayana, M.A. Khan, R. Bhattacharyya, A.K. Pal, Thin Solid Films 472 (2005))180–188.
[15] O.S. Panwar, M.A. Khan, B. Bhattacharjee, A.K. Pal, B.S. Satyanarayana, P.N. Dixit, R. Bhattacharyya, Thin Solid Films 515 (2006) 1597–1606.
[16] Ishpal, O.S. Panwar, A.K. Srivastava, Sushil Kumar, R.K. Tripathi, Mahesh Kumar, Sandeep Singh, Surf. Coat. Technol. 206 (2011) 155–164.

[17] Ishpal, O.S. Panwar, Mahesh Kumar, Sushil Kumar, Mater. Chem. Phys. 125 (2011) 558–567.
[18] O.S. Panwar, Sushil Kumar, Ishpal, A.K. Srivastava, Abhilasha Chouksey, R.K. Tripathi, A. Basu, Mater. Chem. Phys. 132 (2012) 659–664.
[19] R.K. Tripathi, O.S. Panwar, A.K. Srivastava, Ishpal, Mahesh Kumar, Sreekumar Chockalingam, J. Nanosci. 2013 (2013) 401710 (11 pp.).
[20] E.G. Gamaly, T.W. Ebbesen, Phys. Rev. B 52 (1995) 2083–2089.
[21] G.A.J. Amaratunga, M. Chhowalla, C.J. Kiely, I. Alexandrou, R.A. Aharonov, R. Devenish, Nature 383 (1996) 321–323.
[22] M. Chhowalla, R.A. Aharanov, C.J. Kiely, I. Alexandrou, G.A.J. Amaratunga, Philos. Mag. Lett. 75 (1997) 329–335.
[23] I. Alexandrou, C.J. Kiely, A.J. Papworth, G.A.J. Amaratunga, Carbon 42 (2004) 1651–1656.
[24] B.S. Satyanarayana, J. Robertson, W.I. Milne, J. Appl. Phys. 87 (2000) 3126–3131.
[25] O.S. Panwar, M.A. Khan, Satyendra Kumar, A. Basu, B.R. Mehta, Sushil Kumar, Ishpal, Surf. Coat. Technol. 265 (2010) 2126–2133.
[26] Standard data, JCPDS file no. 75-0623.
[27] J. Hu, P. Yang, C.M. Lieber, Phys. Rev. B 57 (1998) 3185–3188.
[28] N. Wada, P.J. Gaczi, S.A. Solin, J. Non-Cryst. Solids 35–36 (1980) 543–548.
[29] S.R. Salis, D.J. Gardiner, M. Bowden, J. Savage, D. Rodway, Diam. Relat. Mater. 5 (1996) 589–591.
[30] A.C. Ferrari, J. Robertson, Phys. Rev. B 61 (2000) 14095–14107.
[31] S. Neuville, A. Matthews, Thin Solid Films 515 (2007) 6619–6653.
[32] H. Sjostrom, S. Stafstrom, M. Boman, J.E. Sundgren, Phys. Rev. Lett. 75 (1995) 1336–1339.
[33] M. Sakai, Acta Metall. Mater. 41 (1993) 1751–1758.
[34] J.F. Lin, P.J. Wei, J.C. Pan, C.F. Ai, Diam. Relat. Mater. 13 (2004) 42–53.
[35] B. Jonsson, S. Hogmark, Thin Solid Films 114 (1984) 257–269.
[36] R. Saha, W.D. Nix, Acta Mater. 50 (2002) 23–38.
[37] X. Chen, J.J. Vassal, J. Mater. Res. 16 (2001) 2974–2982.
[38] H.S. Zhang, K. Komvopoulos, Rev. Sci. Instrum. 79 (2008) 073905 (7 pp.).
[39] J.D. Carey, Philos. Trans. R. Soc. A 361 (2003) 2891–2907.
[40] R.H. Fowler, L. Nordheim, Proc. R. Soc. A 119 (1928) 173–181.
[41] O.S. Panwar, Sushil Kumar, S.S. Rajput, Rajnish Sharma, R. Bhattacharyya, Vacuum 72 (2004) 183–192.
[42] O.S. Panwar, Sushil Kumar, S.S. Rajput, Rajnish Sharma, R. Bhattacharyya, Indian J. Pure Appl. Phys. 41 (2003) 175–182.
[43] O.S. Panwar, Rajnish Sharma, Sushil Kumar, P.N. Dixit, J. Vac. Sci. Technol. B21 (2003) 1986–1995.
[44] O. S. Panwar, M. A. Khan, B. S. Satyanarayana, R. Bhattacharyya, B. R. Mehta, Sushil Kumar, Ishpal, J. Vac. Sci. Technol. B 28 (2010) 411-422.
[45] O.S. Panwar, N. Rupesinghe, G.A. J. Amaratunga, J. Vac. Sci. Technol. A 26 (2008) 566–575.
[46] S. Gupta, B.L. Weiss, B.R. Weiner, G. Morell, J. Appl. Phys. 89 (2001) 5671–5675.
[47] O.S. Panwar, R.K. Tripathi, A.K. Srivastava, Sreekumar Chockalingam, Adv. Sci. Eng. Med. (2014) (in press).
[48] C. Ducati, E. Barborini, P. Pieseri, P. Milani, J. Robertson, J. Appl. Phys. 92 (2002) 5482–5489.
[49] A. Hart, B.S. Satyanarayana, W.I. Milne, J. Robertson, Appl. Phys. Lett. 74 (1999) 1594–1596.
[50] P.M. Koinkar, S.S. Patil, T.-G. Kim, D. Yonekura, M.A. More, D.S. Joag, R.-I. Murakami, Appl. Surf. Sci. 257 (2011) 1854–1858.
[51] N.S. Xu, S.E. Huq, Mater. Sci. Eng. R 48 (2005) 47–189.
[52] K. Lee, V. Scardaci, H.Y. Kim, T. Hallam, H. Nolan, B.E. Bolf, G.S. Maltbie, J.E. Abbott, G.S. Duesberg, Sens. Actuators B 188 (2013) 571–575.
[53] S. Pandey, G.K. Goswami, K.K. Nanda, Sci. Rep. 3 (2013) 2082 (6 pp.).
[54] N. Hu, Z. Yang, Y. Wang, L. Zhang, Y. Wang, X. Huang, H. Wei, L. Wei, Y. Zhang, Nanotechnology 25 (2014) 025502 (9 pp.).
[55] J.M. Tulliani, A. Cavalieri, S. Musso, E. Sardella, F. Geobaldo, Sens. Actuators B 152 (2011) 144–154.
[56] B. Karunagaran, P. Uthirakumar, S.J. Chung, S. Velumani, E.K. Suh, Mater. Charact. 58 (2007) 680–684.